Chalcogenide Letters Vol. 18, No. 12, December 2021, p. 765 - 775

Investigation of the physical properties of nanostructured CO:NiO thin films

M. Ghougali[a], O. Belahssen[b], S. Benhamida[c,*], M. Mimouni[a], G. Rihia[a], M. S. Mahboub[a], A. Beggas[a]
[a]*LEVRES Laboratory, University of El Oued, B.P. 789 39000 El Oued, ALGERIA*
[b]*Physics Laboratory of Thin Films and Applications (LPCMA), University of Biskra, B.P. 145 R.P 07000 Biskra, ALGERIA*
[c]*LRPPS Laboratory, Faculty of Mathematics and Matter Sciences, Kasdi Merbah University, 30000, Ouargla, Algeria*

In this paper, the Co:NiO thin films were deposited on glass substrates under the temperature of (480°C) by spray pyrolysis technique)SPT), and their structural, electrical and optical properties were studied. The films prepared with a molar concentration of 0.2 mol/l from solutions of nickel nitrate and cobalt (II) chloride hexahydrate. The XRD results showed that the films have a fcc structure with preferred orientation (111). The optical band gap energy and Urbach energy were found ranging between 3.61 to 3.48 eV and 0.353 to 0.915 eV respectively. The maximum value of electrical conductivity was 0.08961 Ω-1.cm-1, it was obtained at 12 at.%.

(Received October 30, 2021; Accepted December 6, 2021)

Keywords: Co-doping, NiO thin films, XRD, Optical properties, Electrical conductivity

1. Introduction

In recent years, nanotechnology has boosted ancient fields of knowledge due to the simple reduction of the crystals size. New morphologies or shapes have been created, resulting in improvement in performance or changes in material properties [1]. Nickel oxide (NiO) thin films is among the most comprehensively examined metal oxides. It is a transparent p-type conductive film, which has a NaCl-type structure and it is an antiferromagnetic semiconductor [2, 3]. It offers promising candidates for many applications such as supercapacitors [4], electrochromic devices [5, 6], photo-catalytic [7] and gas sensors [8, 9]. Nickel oxide thin film were prepared by by different techniques including: chemical deposition, electron beam evaporation, magnetron sputtering, sol–gel and spray pyrolysis technique (SPT) [8]. In this work, we chose the spray pyrolysis technique to prepare Co:NiO thin films on glass substrates because it is simple and low cost technique.

2. Materials and preparation

NiO thin films were prepared on a glass substrates (Standard glass CITOPLUS-REF-0302-0004) using SPT. The 5.816 g of nickel (II) nitrate hexahydrate [$Ni(NO_3)_2.6\ H_2O$] was dissolved in100 ml of doubly distilled water to obtain the solution with molar concentration of 0.20 mol/l. Then the 4.758 g of cobalt (II) chloride hexahydrate [$CoCl_2.6\ H_2O$] dissolved in 100 ml of doubly distilled water to obtain the 0.20 mol/l of precursor solution. The two Precursor solutions were stirred at 60°C for half hours in order to obtain a clear and homogenous solution. To obtain the Co/Ni atomic doping ratios, we use certain volume proportions of the precursor solutions calculated from equation (1).

$$\mathrm{Co}(\mathrm{at}\%) = \frac{V_{S_a}}{V_{S_a} + V_{S_b}} \times 100 \tag{1}$$

* Corresponding author: benhamidas9@gmail.com
https://doi.org/10.15251/CL.2021.1812.765

where the precursor solution volume of cobalt (II) chloride dihydrate (V_{Sa}) is added to the precursor solution volume of nickel (II) nitrate hexahydrate (V_{Sb}) for obtain the Co/Ni atomic ratios: 0, 3, 6, 9, 12 at.%. The mixture solution was stirred at 60°C for half an hour to obtain a homogeneous solution. Then, this latter was sprayed onto heated substrates at 480°C. The atomizer-substrate distance was adopted 20 cm, the spray flux was 5 ml/min, each spray takes five second, and the time difference between two successive sprays was 30 second to avoid low substrate temperature. Different precursor solutions of same volume (15 ml) were sprayed fragmentarily to obtain Co:NiO thin films. After deposition operation, the films were left to cool to room temperature.

3. Characterization methods

The XRD patrons of the Co-doped NiO nanostructured thin films prepared were measured to verify its structure. X-ray diffraction was measured using PROTO-MANUFACTURING diffractometer with CuKα radiation (λ= 1.540593Å) operated in the 2θ scanning range from 30° to 80°. The transmittance (T) of the Co:NiO thin films was measured on the wavelength ranging between 200-900 nm using an ultraviolet-visible spectrophotometer (Shmadzu 1800). However, the electrical properties of the simples were measured with keithley model 2400 low voltage source meter. In order to preview the surface morphology properties, the images of the surfaces were taken by a scanning electron microscope (SEM) TESCAN VEGA3. All measurements were achieved at room temperature.

4. Results and discussion

4.1. Structural and morphological properties

Fig. 1 shows the XRD patterns of Co:NiO thin films. It can be seen three main diffraction peaks positioned at 2θ ≈ 37.3°, 43.3° and 79.4° assigned to the (111), (200) and (222) crystal planes respectively. These peaks correspond precisely to the NaCl crystalline structure of NiO and matched well with the standard spectrum (JCPDS, No.47-1049) under the space group Fm3m. The presence of such peaks indicates that the films are polycrystalline in nature. From the XRD analysis, there is secondary phase at 2θ≈39.4° that corresponds to ($60\bar{2}$) peak in cobalt dioxide (CoO_2) can be observed, it is according to JCPDS (No. 98-008-7942), this peak is signalized by a square (■) in Figure 3.23, which could be due to the difference of the ionic radius of the Co and Ni (RNi2+≈ 0.69 Å, RCo2+ ≈ 0.74.5 Å) [10]. This may cause internal stress in the host lattice. It can be attributed to the fact that lower proportion cobalt ions replace nickel ions as substitute, but upon higher doping, more cobalt ions may affect the crystalline structure of films [11].

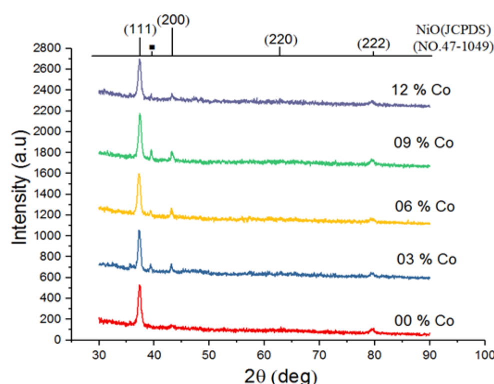

Fig. 1. X-ray diffraction pattern of the Co:NiO thin films.

The intensity of (111) diffraction peak is higher compared with other observed peaks indicating the preferred orientation, its intensity is found to decrease with increasing Co doping percentage rations, this is confirmed by the Texture coefficient values which calculated by the Eq. 2 and they are shown in Fig. 2

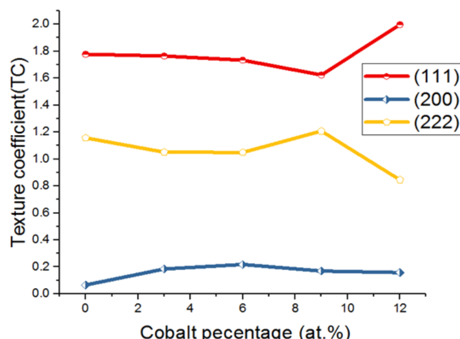

Fig. 2. Texture coefficient values for all peaks of Co:NiO thin films.

Furthermore, we can clearly see from the inset of Fig. 3 that the position of the all diffraction peaks changing with increasing Co-doping percentage. Where, most angle values are shifted to lower values so that the difference Δ(2ϴ)= 2 (ϴ Doped film- ϴ Undoped film) decreases with increasing Co-doping percentage.

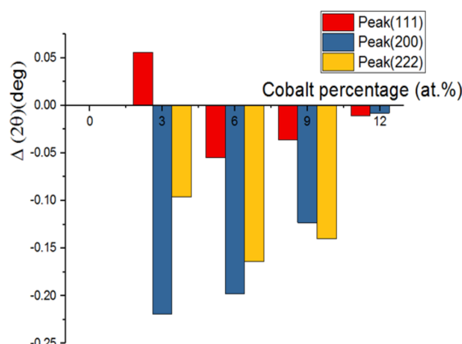

Fig. 3. Variation of the Δ(2ϴ) values as function of Co:NiO thin films.

The texture coefficient (TC) gives the texture in a particular plane, where its difference from unity implies the preferred orientation. The (TC) of the samples were calculated using the Eq. 2 [12]:

$$TC(hkl) = \frac{I(hkl)/I_0(hkl)}{\frac{1}{N}\sum_N I(hkl)/I_0(hkl)} \tag{2}$$

where I(hkl) and I_0(hkl) is the measured intensity and the standard intensity from the JCPDS data based of (hkl) plane respectively, and N is the diffraction peaks number. Generally, the value TC (hkl) = 1 reveals that the films are with randomly oriented grains, while values higher than the unity involve the riches of grains oriented in a given (hkl) direction [12].

Experimentally, the interplanar spacing (d_{hkl}) of various planes were calculated with Bragg's law, using X-rays of known wavelength (λ_0) and measuring Bragg’s angle (θ_{hkl}).

$$d_{hkl} = \frac{\lambda_0}{2\sin\theta_{hkl}} \tag{3}$$

The XRD patterns, were used to calculate the average crystallite sizes (D_{hkl}) of the film in a given direction (hkl), depending on the Scherrer's formula given as [13, 14]:

$$D_{hkl} = \frac{0.9\ \lambda_0}{\beta_{hkl}\cos(\theta_{hkl})} \tag{4}$$

where (λ_0) is the wave length of the X-ray beam, (β_{hkl}) is the full width at half maximum intensity of the peak (hkl) and (θ_{hkl}) is the measuring Bragg's angle.

The experimental lattice parameter values (a_{hkl}) for Cubic systems can be calculated from the following equation using the (hkl) parameters and the interplanar spacing (d_{hkl}) [15].

$$a_{hkl} = d_{hkl}\sqrt{h^2 + k^2 + l^2} \tag{5}$$

The lattice parameters are substrate dependent. This gives increment to a mismatch between the substrate and the deposited NiO films. The latter is responsible of the resulting strains and stresses. The strain (ε) values of the films were estimated from the observed shift, in the diffraction peak between their positions in the XRD spectra via the formula [16, 17]:

$$\varepsilon = (a_{hkl} - a_{hkl}^{o}) / a_{hkl}^{o} \tag{6}$$

where (ε) is the mean strain in thin films, (a_{hkl}) is the lattice constant of thin films and (a_{hkl}^{o}) is the lattice constant of the bulk material, it is taken from the JCPDS card (No. 98-008-7942).
The dislocation is an intra-crystal defect associated with deformation in the periodicity of the crystal lattice of a solid. In contrast to interstitial atoms and vacancies, thermodynamic considerations are insufficient to explain the inclusion of dislocations as a matter of interest [18]. The dislocation density indicates to the number of dislocation lines per unit area of the crystal and is calculated using the following formula [19, 20]:

$$\delta = 1/D^2 \quad \left(\text{Lines/m}^2\right) \tag{7}$$

The crystallite size, interplanar spacing, lattice constants, mean strain and dislocation density of NiO thin films has been calculated using equations (3), (4), (5), (6) and (7) respectively and included in table 1.

From table 1 it can be observed that, the lattice parameter value from undoped film is smaller than to the bulk standard lattice parameter, but for Co-doped films the lattice parameter value is greater (a_0=4.177 Å).

Table 1. Structural parameters of Co:NiO thin films.

Co Concentration (%)	**Lattice constant (Å)**	**Crystallite size *D* (*nm*)**	**Mean strain *ε* (%)**	**Dislocation density δ(lines/m^2).10^{16}**
0	4.169	31.890	-0.186	0.098
3	4.179	40.132	0.041	0.062
6	4.187	33.644	0.247	0.088
9	4.178	53.672	0.032	0.035
12	4.187	48.318	0.016	0.043

Generally, this variation in lattice parameter corresponds to the existence of internal strain, defects or impurities in the films. In this case, the doping leads to the expansion of NiO lattice parameter, which Likely to be due to the difference of the ionic radius of the Co and Ni.the negative sign of the mean strain expression means that the strain is a compressive strain [20]. Conversely, the positive sign means it is an extensive strain and therefore we will use the absolute value in the Fig. 3.

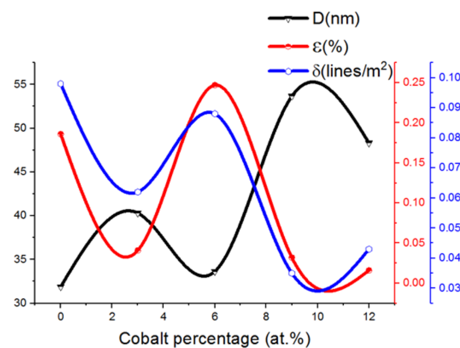

Fig. 4. Correlation between crystallite size, mean strain and dislocation density of Co:NiO thin films

Fig. 4 shows the negative effect of crystalline defects such as strains and dislocations on crystallite size at different doping rates of Co. There is a clear correlation between changes in mean strain and dislocation, which negatively affected the crystallization of the films prepared.

From the Fig. 5 it can be observed that the doping has improved crystallization by increasing the crystallite size with varying values, which positively affects the lattice constant. The latter shows values close to the theoretical value whenever the crystallite size is large.

The films surfaces were studied by scanning electron microscopy (SEM). SEM micrographs were taken for thin films of undoped and Co-doped NiO at 3, 6, 9 and 12 at.% are embedded in Fig.6. The SEM images revealed films show that the deposited films have relative homogeneity on its surface; the shape of the grains and aggregates of grains boundaries does not appear clearly, where the surfaces of the undoped and Co-doped NiO films have a wrinkle network structure. This morphology appears to be clearer and denser as the cobalt concentration increases.

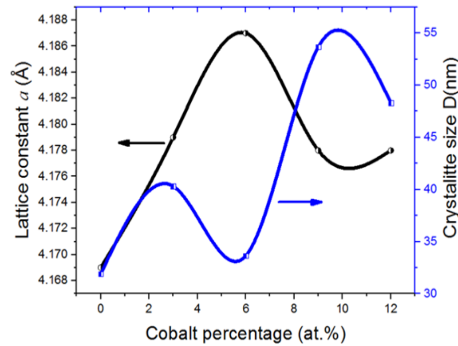

Fig. 5. Variation of crystallite size and lattice constant of Co:NiO thin films

In general, the surfaces of the prepared Co:NiO thin films have a wrinkle lattice structure, and are influenced by the incorporation of Co doping. The incorporation of Cobalt ions into the NiO lattice modified the surface morphology of the films, due to the more impurities included in the NiO lattice structure. The morphology of the structure observed in Co:NiO films can be attributed to the fact that Co dopant promotes nucleation and growth in certain directions at random.

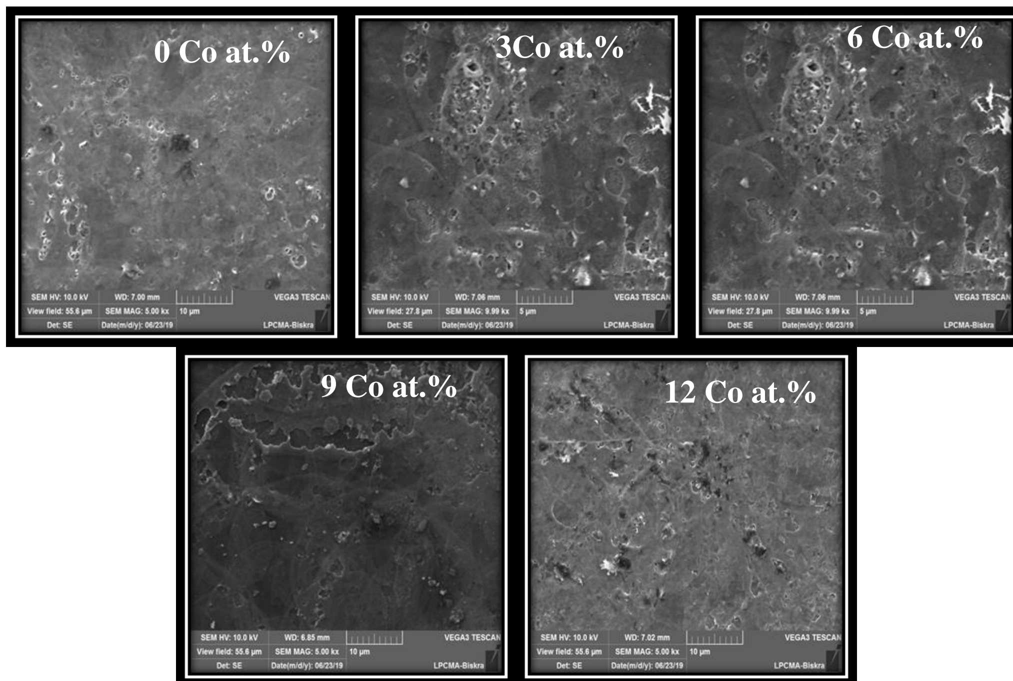

Fig. 6. SEM images of Co:NiO thin films.

4.4. Optical properties

Fig. 7 shows the transmittance spectra in the UV-Visible range (300-900 nm) of Co:NiO thin films in the doping range of 0 to 12 at.%. The figure shows a significant increase in the transmittance values of all thin films with the increase in wavelength in the range (300 - 375 nm), i.e. near the absorption edge, then it increases slowly at higher wavelengths. The spectrum of transmittance shows a relatively low (45-55%) in the range of the visible and near infrared regions. The low transmittance of all samples may be due to the surface roughness of the films as indicated by SEM, and this leads to the scattering of radiation in several directions, which reduces the percentage of transmittance. In the range of (375-650 nm), we observed a significant reduction in

the transmittance values of the doped films compared to the pure sample, but after 650 nm, the transmittance values of the doped films improved to exceed the transmittance of pure sample, that for samples 6 and 12 at.%.

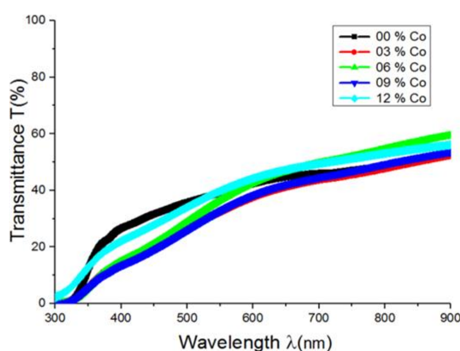

Fig. 7. Transmittance of Co:NiO thin films.

As in transmittance, the absorbance was calculated and studied in the range of (300-900 nm). Fig. 8 shows the variation of absorbance (A) of the Co:NiO thin films as function of wavelength. The absorbance decreases sharply near the edge of the main absorbance, which is in the UV region. Increasing the wavelength decreases the energy of the incident photons and this decrease the concentration of electrons that have enough energy to occur direct electronic transitions, thus limiting the basic absorption in the visible region. Although the nickel oxide has a wide band gap, the prepared films show remarkable absorption in the visible region. Although the nickel oxide has a large band gap, the prepared films show remarkable absorption in the visible region. Three explanations can be proposed for this. The first is the presence of a secondary phase of cobalt oxide CoO_2, it was indicated by XRD, or the presence of Ni_2O_3 as a weak phase that was not detected by XRD [21]. The second possibility is that two adjacent divalent nickel ions become trivalent due to the presence of nickel vacancies where the charge transfer process takes place. The third possibility is the presence of excess oxygen combined with hydrogen forming OH groups that may show significant absorption in the visible region of the spectrum [22].

In general, the band gap energy values depend on the structural properties of the crystallized films (disorder and its regularity) [23]. The direct optical band gap energy of all samples is determined using the Tauc's relationship [24, 25].

$$(\alpha h\nu)^2 = \Gamma\left(h\nu - E_g\right) \tag{8}$$

where (Γ) is a constant, is the optical band gap energy.

Fig. 9 shows $(\alpha h\nu)^2$ as a function of hν for the Co:NiO thin films at various cobalt doping percentage. The statement highlights the linear nature of $(\alpha h\nu)^2$ next to the absorption edge indicating a direct transition between the valence band and the conduction band. Hence, this linear relationship is a clear indication that the material is direct band gap semiconductor. From Fig. 9, can be observe the intersection of the extrapolation of the straight-line portion of the absorption spectrum with the energy axis at the zero absorption coefficients [26].

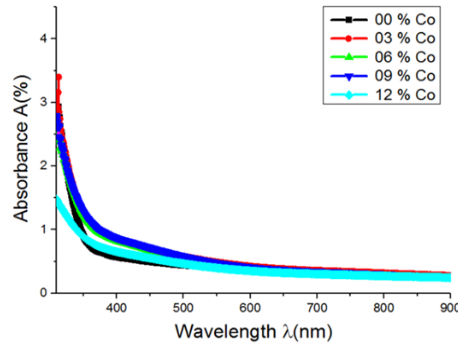

Fig. 8. Absorbance of Co:NiO thin films.

The values of energy at this intersection points indicates the energy of the band E_g, where Its values were summarized in table 2. The values of band gap Eg is 3.61 eV for undoped sample, whereas the values of E_g gradually decreases from 3.60 to 3.48 eV for Co-doped samples from 3 to 12 at.%. This is in good agreement with previous research reports by different groups [27, 28], where they found that the bandgap of NiO films varies between 3.4 eV and 4.0 eV. The band gap is found to decrease with an increase in the Co doping concentration; this suggests a change in the NiO electronic structure i.e the suggests a change in the crystallite growth, defects or vacancies in the NiO crystal which can create new energy levels. This comportment leads to the diminution in the values of the band gap energy [29].

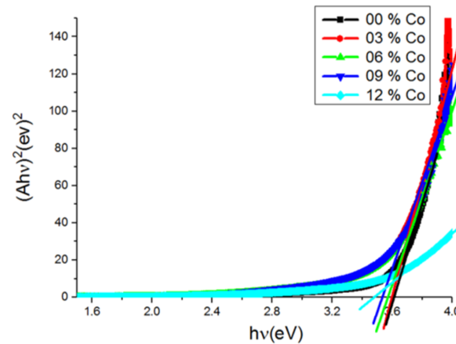

Fig. 9. Plot of $(\alpha h\nu)^2$ versus incident photon energy (hv) of Co:NiO thin films.

At near the absorption band edge, the exponential tail length of the edge is characterized by an energy called Urbach energy (E_U). It is indicating the width of band tails of the localized states within the optical band gap and is given by equation 9 [30].

$$\ln\alpha = \frac{1}{E_U}(hv) + \ln\alpha_0 \tag{9}$$

where is the pre-exponential factor, (hv) the photon energy and (E_U) is the Urbach energy; it is the width of the band tail is related to the the structural defects, density of dislocations and some defects of the interstitial states and vacancy in the films [30-32]. The Urbach energy, can be determined from the inverse slope of the linear plot of with (hv) as represented in Fig. 10. In the case of doped NiO films. Cobalt ions can create more number of localized states that reduce the energy gap under the influence of the Roth effect. Urbach energy values are summarized in Table 2. It is clear that its values increase if the ratio of co-doping increases in contrast to the energy gap values as shown in Fig. 11.

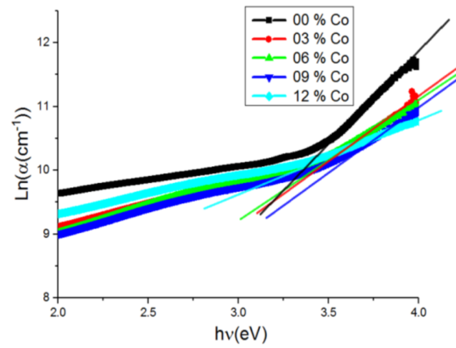

Fig. 10. Plot of Ln(α) versus incident photon energy (hν) of Co:NiO thin films.

Table 2. Optical and electrical parameters of Co:NiO thin films.

Co concentration %	Thickness t(nm)	Optical gap energy E_g (eV)	Urbach energy E_u(meV)	Conductivity σ (Ω.cm)$^{-1}$
0	264	3.61	0.353	0.0169
3	288	3.60	0.531	0.0730
6	269	3.57	0.641	0.0157
9	268	3.56	0.655	0.0240
12	305	3.48	0.915	0.0690

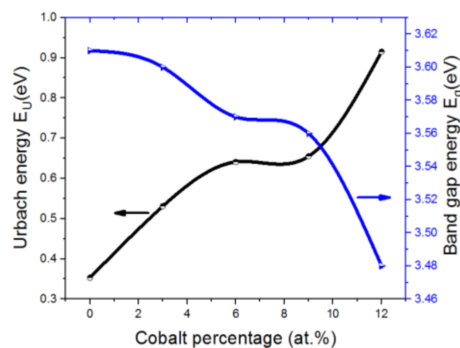

Fig. 11. Reverse correlation between optical band gap energy and Urbach energy of Co:NiO thin films.

4.5. Electrical properties

The conductivity of Co:NiO thin films was measured using the four probe method Depending on the following relationship.

$$\frac{1}{\sigma} = \rho = \frac{\pi}{\ln 2}\, t\, \frac{V}{I} = 4.53236\, t\, \frac{V}{I} \tag{10}$$

where is the conductivity, is the resistivity, is the thickness of th film, is the current and the voltage. The variation of the conductivity versus Co doping of the Co:NiO thin films is shown in Fig. 12. It was clear that the Co:NiO thin films are affected by doping. The films showed high electrical conductivity ranging between 0.0157 and 0.0730 (Ω·cm)$^{-1}$ at the percentage of 6 and 3 at.% respectively. Generally, the electrical conductivity of NiO films has a strong correspondence on the microstructural defects existing in crystallites of NiO, such as interstitial defects, nickel vacancies, therefore the conductivity of films depend strongly on surface effects, the grain size and the boundaries between them [33, 34].

Fig. 12 also shows the close correlation between crystallite size and thickness of films with electrical conductivity, which is clearly affected in case of increasing or decreasing. Except in

the case of doping 12 at. %, which suggests that the effect of thickness in this case is more important than the effect of the crystallite size of films.

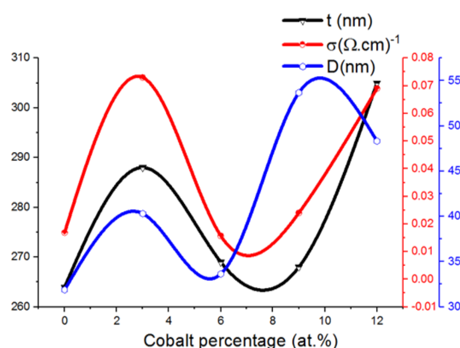

Fig. 12. The variation of crystallite size, thickness of films and electrical conductivity of Co:NiO thin films.

5. Conclusion

Thin films of Co:NiO at 0, 3, 6, 9 and 12 at.% of Co doping were successfully deposited on glass substrates at a temperature of 480°C by SPT. The effect of Co-doping on physical properties of NiO films was investigated. XRD characterization revealed that the Co:NiO thin films have a FCC (NaCl) polycrystalline structure with a preferential orientation (111) and without obvious effect of doping concentration on the positions of the peaks. XRD results indicated also the presence of a secondary phase corresponding to the peak of the cobalt dioxide (CoO2). The crystallite size ranged from the 31.89 to 53.67 nm. SEM images showed that the surfaces of the deposited films have a wrinkle in the lattice structure and it was influenced by the incorporation of Co dopants. UV-VIS revealed that a decrease in the average optical transmission of the films with increasing in the Co concentration. The optical band gap energy was found to have decreased from 3.61 to 3.48 eV and the Urbach energy was found to have increased from 0.353 to 0.915 eV with increasing the Co dopant concentration from 0 to 12 at.%. The maximum value of electrical conductivity was 0.08961 Ω-1.cm-1, it is obtained at 12 at.%.

References

[1] M. Vidotti, R.Salvador, S. Cordobadetorresi, Ultrasonics Sonochemistry **16**, 35 (2009).
[2] P. S. Patil, L. D. Kadam, Applied Surface Science **199**, 211 (2002).
[3] S. Baran, A. Hoser, B. Penc, ACTA Physica Polonica A **129**, 35 (2016).
[4] I. D. Farrukh, R. M. Kevin, E. S. Mohammed, J. Nanoscale Research Letters **8**, 363 (2013).
[5] V. Julijana, P. G. Margareta, N. Metodija, S. Nace, Silpakorn U Science & Tech J. **5**, 34 (2011).
[6] J. S. Anandh, M. Haris, P. Immanuel, Method Int. J. Science and Research **23**, 58 (2014).
[7] A. A-G. Attieh, M. S. Abdel-wahabab, A. A. Farghalibc, P. M. Z. Hasana, Materials Research Bulletin **75**, 71 (2016).
[8] M. S. Amir, J. H. Ahalapitiya, S. Gamini, Applied Surface Science **276**, 291 (2013).
[9] D. G. Enrico,M. Alessandro, Sensors **15**, 16910 (2015).
[10] F. N. Al. Shammary, Journal of Kufa – Physics **2**, 22 (2010).
[11] S. Sriram, A. Thayumanavan, International Journal of Materials Science and Engineering **1**, 118 (2013).
[12] S. Ilican, M. Caglar, Y. Caglar, Materials Science-Poland **25**709, (2007).
[13] V. Saravanakannan, T. Radhakrishnan, International Journal of ChemTech Research **6**, 306 (2014).

[14] A. Rahdar, M. Aliahmadb, Y. Azizi, Journal of Nanostructures **5**, 145 (2015).
[15] L. Cattin, B. A. Reguig, A. Khelil, M. Morsli, K. Benchouk, J. C. Bernede, Applied Surface Science **254**, 5814 (2008).
[16] O. Belahssen, M. Ghougali, A. Chala, Journal of Nano-and Electronic Physics **10**, 1 (2018).
[17] M. Mekhnache, A. Drici, L. S. Hamideche, H. Benzarouk, A. Amara, L. Cattin, J. C. Bernede, M. Guerioune, Superlattices and Microstructures **49**, 510 (2011).
[18] A. F. Saleh, International Journal of Application or Innovation in Engineering & Management **2**, 16 (2013).
[19] M. Karunakaran, S. Maheswari, K.Kasirajan, S. Dineshraj, International Journal for Research in Applied Science & Engineering Technology **4**, 691 (2016).
[20] Y. Z. Dawood, M. H. Hassoni, M. S. Mohamad, International Journal of Pure and Applied Physics **2**, 1 (2014).
[21] N. A. Bakr, S. A. Salman, A. M. Shano, Physics and Astronomy **2**, 15 (2015).
[22] P. S. Patil, L. D. Kadam, Applied surface science **199**, 211 (2002).
[23] M. N. Armenise, C. E. Campanella, C. Ciminelli, F. Dell'Olio, V. M. N. Passaro, Physics Procedia **3**, 357 (2010).
[24] F. N. Al. Shammary, Journal of Kufa – Physics **2**, 22 (2010).
[25] S. Sriram, A. Thayumanavan, International Journal of Materials Science and Engineering **1**, 118 (2013).
[26] N. N. Jandow, International Letters of Chemistry, Physics and Astronomy **48**, 155 (2015).
[27] O. K. Ukoba, F. Inambao, A. E. Eboka, Energy Procedia **142**, 244 (2017).
[28] M. Ghougali, O. Belahssen, A. Chala, Journal of Nano-Electron. Physics **10**, 1 (2018).
[29] S. I. Abbas, A. Q. Ubaid, Journal of Advances in physics **6**, 1016 (2014).
[30] F. N. C. Anyaegbunam, C. Augustine, Digest Journal of Nanomaterials and Biostructures **13**, 847 (2018).
[31] K. Anandan, V. Rajendran, International Journal of Advanced Trends in Engineering and Technology **2**, 1 (2017).
[32] F. Al-Shaikley, Indian Journal of Applied Research **3**, 544 (2013).
[33] W. Zhang, S. H. Brongersma, T. Clarysse, V. Terzieva, E. Rosseeel, W. Vandervorst, K. Maex, Journal of Vacuum Science & Technology B: Microelectronics and Nanometer Structures **22**, 1830 (2004).
[34] F. D. Paraguay, L. W. Estrada, N. D. R. Acosta, E. Andrade, M. M. Yoshida, Thin Solid Films **350**, 192 (1999).